

Article

# Design of Static Output Feedback Suspension Controllers for Ride Comfort Improvement and Motion Sickness Reduction

Jinwoo Kim and Seongjin Yim \* 

Department of Mechanical and Automotive Engineering, Seoul National University of Science and Technology, 232 Gongneung-ro, Nowon-gu, Seoul 01811, Republic of Korea; king@g.seoultech.ac.kr

\* Correspondence: acebtif@seoultech.ac.kr; Tel.: +82-2-970-9011

**Abstract:** This paper presents a method to design a static output feedback active suspension controller for ride comfort improvement and motion sickness reduction in a real vehicle system. Full-state feedback controller has shown good performance for active suspension control. However, it requires a lot of states to be measured, which is very difficult in real vehicles. To avoid this problem, a static output feedback (SOF) controller is adopted in this paper. This controller requires only three sensor outputs, vertical velocity, roll and pitch rates, which are relatively easy to measure in real vehicles. Three types of SOF controller are proposed and optimized with linear quadratic optimal control and the simulation optimization method. Two of these controllers have only three gains to be tuned, which are much smaller than those of full-state feedback. To validate the performance of the proposed SOF controllers, a simulation is carried out on a vehicle simulation package. From the results, the proposed SOF controllers are quite good at improving ride comfort and reducing motion sickness.

**Keywords:** active suspension; ride comfort; motion sickness; full-state feedback; static output feedback; linear optimal control; simulation-based optimization



**Citation:** Kim, J.; Yim, S. Design of Static Output Feedback Suspension Controllers for Ride Comfort Improvement and Motion Sickness Reduction. *Processes* **2024**, *12*, 968. <https://doi.org/10.3390/pr12050968>

Academic Editor: Gorazd Karer

Received: 14 April 2024

Revised: 9 May 2024

Accepted: 9 May 2024

Published: 9 May 2024



**Copyright:** © 2024 by the authors. Licensee MDPI, Basel, Switzerland. This article is an open access article distributed under the terms and conditions of the Creative Commons Attribution (CC BY) license (<https://creativecommons.org/licenses/by/4.0/>).

## 1. Introduction

To date, ride comfort and road handling have been regarded as two objectives to be satisfied in suspension design and control [1,2]. The vertical acceleration,  $a_z$ , of a sprung mass (SPM) has been used as a measure for ride comfort. On the other hand, tire deflection has been used as a measure for road handling. Figure 1 shows ISO2631-1, which represents the sensitivity of human bodies to frequency ranges in the vertical and horizontal directions [3,4]. As shown in Figure 1, the frequency range of  $a_z$  related to ride comfort,  $W_k$ : vertical, is 4.0~10.0 Hz. For this reason,  $a_z$  within this range should be reduced by suspension control for ride comfort [4].

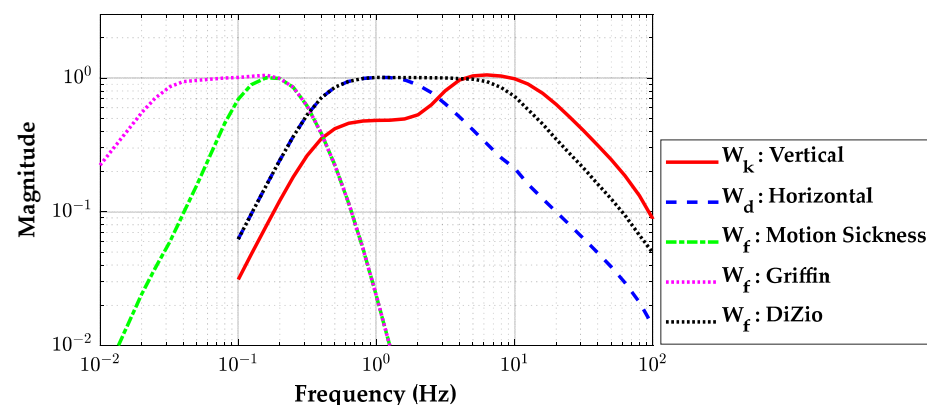


**Figure 1.** Frequency weightings specified in ISO 2631 [3] and proposed by Griffin and Dizio.

Since the early 2010s, autonomous driving has been intensively studied [5]. Autonomous driving or advanced driving assistance systems (ADAS) can make passengers engage in non-driving-related visual tasks such as having a coffee, checking emails, and reading a book or display devices [6–8]. This is a key advantage of autonomous driving. However, it can make motion sickness severe compared to conventional manual driving. For this reason, different from the studies on conventional suspension control for ride comfort, motion sickness should be taken into account when developing autonomous driving function.

For more than a decade, it has been known that motion sickness is caused by vertical vibration within the range of 0.1~0.2 Hz, shown as **W<sub>f</sub>: Motion Sickness** in Figure 1. This was obtained from the vibration on a ship. In the early 2000s, the studies carried out by Griffin showed that this range covers the range of 0.03~0.2 Hz, shown as **W<sub>f</sub>: Griffin** in Figure 1 [7,9–13]. For the last decade, studies investigating motion sickness on driving have shown that motion sickness is easily caused by combined  $a_z$ , pitch and roll rates ( $\dot{\theta}$  and  $\dot{\phi}$ ) in the 0.8~8.0 Hz range, shown as **W<sub>f</sub>: DiZio** in Figure 1 [14,15]. This is overlapped with **W<sub>k</sub>: vertical**, 4.0~10.0 Hz. A comprehensive literature review on motion sickness can be found in reference [16]. For this reason,  $a_z$ ,  $\dot{\theta}$  and  $\dot{\phi}$  of an SPM over the range of 0.8~8.0 Hz should be reduced in order to improve ride comfort and to reduce motion sickness. For the purpose of the previous study, those variables of an SPM were controlled with active suspension and the SOF control method [17].

To date, several types of actuators have been used to control the suspension in vehicles such as active suspension and magneto-rheological (MR) damper. Among those actuators, active suspension control (ASC) has been intensively studied because it is quite an effective actuator for improving ride comfort and road handling. A literature survey on ASC was given in [1,2,18–20]. Recent developments over the last decade in the area of ASC are reviewed in [21]. In this paper, active suspension is adopted as an actuator, which is needed to generate a vertical force in a suspension.

To improve ride comfort and to reduce motion sickness, the vertical, roll and pitch (VRP) motions ought to be controlled by a controller. For this purpose, a vehicle model describing those motions is needed. To date, quarter-, half- and full-car models have been selected for controller design [19]. Among those models, a full-car model can describe the VRP motions of an SPM. For this reason, a full-car model is used as vehicle one in this paper. From this model, a linear state-space equation (SSE) is derived. In case there are nonlinear springs and dampers in a suspension, a Simulink model is built to describe their nonlinear behavior for simulation optimization (SLOM) [17].

To date, for ASC, various controller design methods such as linear quadratic optimal control (LQOC), adaptive and nonlinear control methods have been applied [22–25]. Among those methods, the linear quadratic regulator (LQR) is the most commonly used method for ASC because it is systematic and easy to tune [20]. LQR is a full-state feedback controller, which needs all system states to be measured or estimated for feedback. For instance, quarter-, half- and full-car models have 4, 8 and 14 state variables and one, two, and four control inputs, respectively. As a result, the gain matrices of LQR for quarter-, half- and full-car models have the dimensions of  $1 \times 4$ ,  $2 \times 8$ , and  $4 \times 14$ , respectively. For the full-car model, LQR is too large to be implemented in a real vehicle. Moreover, it is very difficult to measure all system states in a real vehicle, and, consequently, LQR is very hard to implement on a real vehicle. To resolve this problem, two solutions have been adopted. The first is to use a state observer or Kalman filter to estimate state variables from sensor signals [22–24]. However, the parameters of a model should be known exactly a priori for a state observer. Moreover, a state observer requires an extra design procedure besides LQR. Instead of a state observer, the second is to use a static output feedback (SOF) control with available sensor signals in real vehicles [17,26–29]. Especially important, previous studies have only used two gains in the linear quadratic SOF (LQSOF) controller for the full-car model [28,29]. For this reason, SOF control is adopted as a controller structure in this paper.

In this paper, the vertical velocity ( $v_z$ ), roll and pitch rates ( $\dot{\theta}$  and  $\dot{\phi}$ ) of the SPM are selected as an available output for the SOF controller. In the full-car model, there are four control inputs. As a result,  $4 \times 3$  gains are needed for the SOF controller. Besides the SOF controller with 12 gains in this paper, from the symmetry between roll and pitch motions of the SPM, two types of SOF controllers are proposed, which have only three gains [17]. These SOF controllers are much easier to implement in a real vehicle because they have a much smaller number of gains. Moreover, it is also easier to optimize these controllers.

To design or optimize the SOF controller, linear quadratic optimal control (LQOC) and the simulation optimization method (SLOM) are adopted in this paper. LQOC uses the SSE and LQ cost function for controller design. In LQOC, an LQ cost function is derived from the state variables and minimized by a heuristic optimization method [28,29]. SLOM uses the Simulink model with nonlinear springs and dampers and a cost function defined for improving ride comfort and reducing motion sickness. The Simulink model is built from the full-car model, and the cost function is evaluated from the results of the Simulink model and optimized by a heuristic optimization method (HOM) [17,30]. As a HOM for optimization, the covariance matrix adaptation evolution strategy (CMA-ES) is selected in this paper [31]. To check the control performance of the controllers designed by LQOC and SLOM, a simulation is performed on the vehicle simulation package, CarSim. By analyzing the simulation results, it is identified which controller is the best for ride comfort improvement and motion sickness reduction.

The objective of this paper is to design SOF active suspension controllers with LQOC and SLOM for the purpose of improving ride comfort and reducing motion sickness. The contributions of this paper can be summed up as follows:

1. Three types of structures of SOF controllers are presented. With  $v_z$ ,  $\dot{\theta}$  and  $\dot{\phi}$  of an SPM as an output, three SOF control structures are presented. Those signals for the SOF controllers are obtained by integrating the vertical accelerations measured at each corner of the SPM.
2. To design a SOF controller for a nonlinear vehicle model, SLOM is applied. Simulink model for the nonlinear vehicle one is built and the SOF controllers are optimized with SLOM.
3. With the designed SOF controllers, a simulation is conducted on CarSim for comparison. Based on simulation results, it is recommended which SOF controller is the best for ride comfort improvement and motion sickness reduction.

This paper comprises four sections. In Section 2, a full-car model is presented and its SSE is derived. From the geometry of the SPM, three types of SOF control structures are proposed and designed with LQOC and SLOM. In Section 3, frequency response analysis and a simulation are conducted on CarSim. The conclusions are drawn in Section 4.

## 2. Design of Static Output Feedback Controllers

In this section, the SSE for the full-car models is derived, as presented in previous studies [17,28,29,32,33]. With the SSE, LQR and LQSOFC controllers are designed. For a vehicle with nonlinear spring and damper, a vehicle model is built with MATLAB/Simulink (version: 9.6.0.1472908, R2019a, The MathWorks Inc., Natick, MA, USA), and SLOM is applied to design SOF controllers.

### 2.1. Full-Car Model and State-Space Equation

Figure 2 shows a free-body diagram of the full-car model, which has four suspensions,  $S_1$ ,  $S_2$ ,  $S_3$  and  $S_4$ . In the model, there are seven motions: three motions for the SPM and four motions of the unsprung mass (USPM). For the SPM, the VRP motions are described by three corresponding variables, i.e., the vertical displacement,  $z_c$ , the roll angle,  $\phi$ , and the pitch angle,  $\theta$ , respectively. In the SPM, the vertical displacements at each corner are described by  $z_s$ , which is determined by the geometry of the SPM and three variables,  $z_c$ ,  $\phi$  and  $\theta$ . For the USPM, the vertical motions are described by the vertical displacement,  $z_u$ .

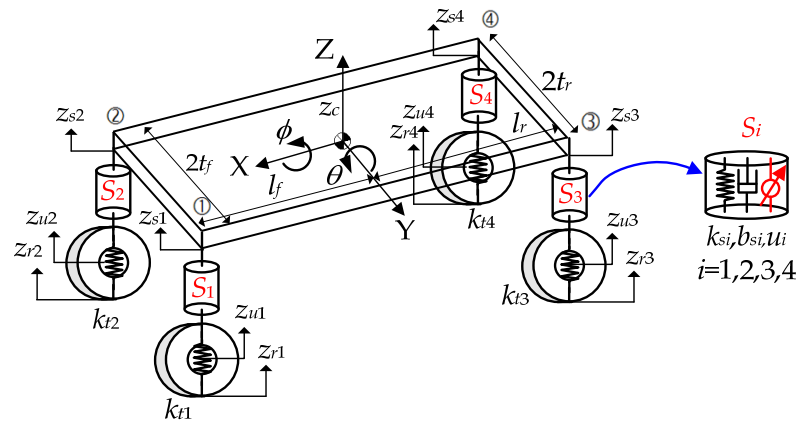


Figure 2. Free-body diagram of 7-DOF full-car model.

As shown in Figure 2, each suspension  $S_i$  has a spring of stiffness  $k_{si}$ , a damper of damping coefficient  $b_{si}$  and control input  $u_i$  generated by an actuator. An active actuator is installed alongside a spring and a damper in a suspension. Those four actuators can generate the control inputs,  $u_1, u_2, u_3$  and  $u_4$ , at each suspension. A controller calculates those control inputs from the variables describing the motions of the SPM and USPM.

In the full-car model, three motions of the SPM and four motions of the USPM are excited by four disturbances, i.e., the road profiles,  $z_{r1}, z_{r2}, z_{r3}$  and  $z_{r4}$ , which are applied to the USPM. Generally, the disturbances exciting on the front USPMs do act on the rear ones in some delay. The delay between the front and rear suspensions depends on vehicle speed.

In the suspension  $S_i$ , the suspension force  $f_i$  is calculated as in Equation (1). In Equation (1),  $u_i$  is the control input generated by an actuator in  $S_i$ . To derive a linear equation, the cubic terms in (1) are neglected. With those, three and four equations of motions for the SPM and USPM are derived as Equations (2) and (3), respectively. Assuming that there are no longitudinal and lateral motions for the SPM, i.e.,  $v_x = v_y = 0$ , and that the cross moments of inertia,  $I_{xy}, I_{xz}$  and  $I_{yz}$ , can be neglected, Equation (2) is linearized as (4). Equation (4) is obtained as Equation (5). Hereafter, the matrix  $\mathbf{H}$  plays an important role in this paper.

$$f_i = -\left\{k_{si}(z_{si} - z_{ui}) + k_{ci}(z_{si} - z_{ui})^3\right\} - \left\{b_{si}(\dot{z}_{si} - \dot{z}_{ui}) + b_{ci}(\dot{z}_{si} - \dot{z}_{ui})^3\right\} + u_i, \quad i = 1 \dots 4 \quad (1)$$

$$\begin{cases} m_s(\ddot{z}_c - \dot{\theta}v_x + \dot{\phi}v_y) = f_1 + f_2 + f_3 + f_4 \\ I_x\ddot{\phi} + I_{xy}\ddot{\theta} + I_{xz}\dot{\phi}\dot{\theta} + I_{yz}\dot{\theta}^2 = t_f \cdot (f_1 - f_2) + t_r \cdot (f_3 - f_4) \\ I_y\ddot{\theta} + I_{xy}\dot{\phi} - I_{yz}\dot{\phi}\dot{\theta} - I_{xz}\dot{\phi}^2 = -l_f \cdot (f_1 + f_2) + l_r \cdot (f_3 + f_4) \end{cases} \quad (2)$$

$$m_{ui}\ddot{z}_{ui} = k_{ti}(z_{ui} - z_{ri}) - f_i, \quad i = 1, 2, 3, 4 \quad (3)$$

$$\begin{cases} m_s\ddot{z}_c = f_1 + f_2 + f_3 + f_4 \\ I_x\ddot{\phi} = t_f \cdot (f_1 - f_2) + t_r \cdot (f_3 - f_4) \\ I_y\ddot{\theta} = -l_f \cdot (f_1 + f_2) + l_r \cdot (f_3 + f_4) \end{cases} \quad (4)$$

$$\begin{bmatrix} m_s\ddot{z}_c \\ I_x\ddot{\phi} \\ I_y\ddot{\theta} \end{bmatrix} = \underbrace{\begin{bmatrix} 1 & 1 & 1 & 1 \\ t_f & -t_f & t_r & -t_r \\ -l_f & -l_f & l_r & l_r \end{bmatrix}}_{\mathbf{H}} \underbrace{\begin{bmatrix} f_1 \\ f_2 \\ f_3 \\ f_4 \end{bmatrix}}_{\mathbf{f}} = \mathbf{H}\mathbf{f} \quad (5)$$

In Equation (1), the vertical displacements and velocities of the SPM at each corner,  $z_{si}$  and  $\dot{z}_{si}$ , are not a state variable. So, it is to be represented with the state variables, i.e.,  $z_c, \phi$  and  $\theta$ . Figure 3 shows how to calculate the vertical displacements of the SPM at four corners, i.e., ①, ②, ③ and ④ in Figure 2. As shown in Figure 3,  $z_{s1}, z_{s2}, z_{s3}$  and  $z_{s4}$  are

derived as in Equation (6) from the geometry of the SPM. In Equation (6), the nonlinear terms are approximated as  $\sin\theta \approx \theta$  and  $\sin\phi \approx \phi$  assuming that  $\phi$  and  $\theta$  are small. With this approximation, Equation (6) is rearranged into Equation (7) [28,29,32,33]. In Equation (7), the matrix  $\mathbf{H}$  stands for the geometric relationship among four variables,  $z_{s1}$ ,  $z_{s2}$ ,  $z_{s3}$  and  $z_{s4}$ , and the three state variables,  $z_c$ ,  $\phi$  and  $\theta$ .

$$\begin{cases} z_{s1} = z_c + t_f \cdot \sin\phi - l_f \cdot \sin\theta \approx z_c + t_f \cdot \phi - l_f \cdot \theta \\ z_{s2} = z_c - t_f \cdot \sin\phi - l_f \cdot \sin\theta \approx z_c - t_f \cdot \phi - l_f \cdot \theta \\ z_{s3} = z_c + t_f \cdot \sin\phi + l_r \cdot \sin\theta \approx z_c + t_f \cdot \phi + l_r \cdot \theta \\ z_{s4} = z_c - t_f \cdot \sin\phi + l_r \cdot \sin\theta \approx z_c - t_f \cdot \phi + l_r \cdot \theta \end{cases} \quad (6)$$

$$\begin{bmatrix} z_{s1} \\ z_{s2} \\ z_{s3} \\ z_{s4} \end{bmatrix} = \begin{bmatrix} 1 & t_f & -l_f \\ 1 & -t_f & -l_f \\ 1 & t_f & l_r \\ 1 & -t_f & l_r \end{bmatrix} \begin{bmatrix} z_c \\ \phi \\ \theta \end{bmatrix} = \mathbf{H}^T \begin{bmatrix} z_c \\ \phi \\ \theta \end{bmatrix}, \quad \begin{bmatrix} \dot{z}_{s1} \\ \dot{z}_{s2} \\ \dot{z}_{s3} \\ \dot{z}_{s4} \end{bmatrix} = \mathbf{H}^T \begin{bmatrix} \dot{z}_c \\ \dot{\phi} \\ \dot{\theta} \end{bmatrix} \quad (7)$$

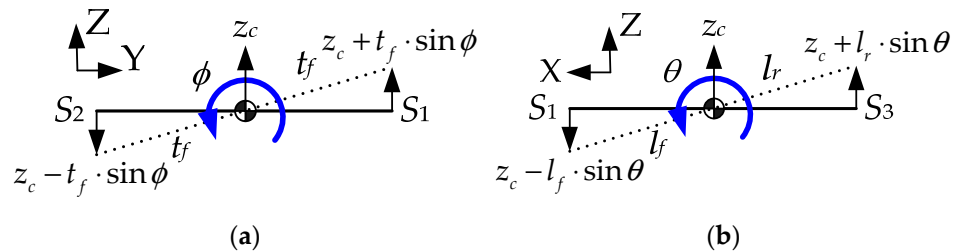


**Figure 3.** Calculation of vertical displacements at four corners of the SPM. (a) Front view; (b) side view.

From the variables and the parameters of the full-car model, new vectors and matrices are defined as in Equations (8) and (9), respectively [28,29,32,33]. With those definitions, Equation (7) is represented as Equation (10). With Equation (10), Equation (1) is represented as Equation (11). With Equations (5), (8) and (9), Equations (3) and (4) are represented as Equation (12). By replacing the  $\mathbf{f}$  of Equation (12) with (11), Equation (12) is transformed into Equation (13). Equation (13) is rearranged into another vector-matrix form as in Equation (14). In Equation (14), the new matrices,  $\mathbf{M}$ ,  $\mathbf{K}$ ,  $\mathbf{B}$ ,  $\mathbf{U}$  and  $\mathbf{L}$  are defined. New vectors,  $\mathbf{z}$  and  $\mathbf{x}$ , are defined as in (15). With those vectors and matrices, Equation (14) is rewritten into Equation (16). Following the above procedure, the equations of motions of the SPM and USPM, Equations (3) and (4), are rearranged into Equation (16). Equation (16) is rearranged into the new vector-matrix form of Equation (17). The state vector  $\mathbf{x}$  of the full-car model is defined as in Equation (15). With the definition of the state vector and Equation (16), the SSE of the full-car model is obtained as in Equation (18).

$$\mathbf{z}_s \triangleq [z_{s1} \quad z_{s2} \quad z_{s3} \quad z_{s4}]^T, \quad \mathbf{z}_u \triangleq [z_{u1} \quad z_{u2} \quad z_{u3} \quad z_{u4}]^T, \quad \mathbf{z}_r = \mathbf{w} \triangleq [z_{r1} \quad z_{r2} \quad z_{r3} \quad z_{r4}]^T \quad (8)$$

$$\mathbf{p} \triangleq [z_c \quad \phi \quad \theta]^T, \quad \mathbf{u} \triangleq [u_1 \quad u_2 \quad u_3 \quad u_4]^T$$

$$\mathbf{M}_s \triangleq \text{diag}(m_s, I_x, I_y), \quad \mathbf{M}_u \triangleq \text{diag}(m_{u1}, m_{u2}, m_{u3}, m_{u4}) \quad (9)$$

$$\mathbf{K}_s \triangleq \text{diag}(k_{s1}, k_{s2}, k_{s3}, k_{s4}), \quad \mathbf{K}_t \triangleq \text{diag}(k_{t1}, k_{t2}, k_{t3}, k_{t4}), \quad \mathbf{B}_s \triangleq \text{diag}(b_{s1}, b_{s2}, b_{s3}, b_{s4})$$

$$\mathbf{z}_s = \mathbf{H}^T \mathbf{p}, \quad \dot{\mathbf{z}}_s = \mathbf{H}^T \dot{\mathbf{p}} \quad (10)$$

$$\mathbf{f} = -\mathbf{K}_s(\mathbf{z}_s - \mathbf{z}_u) - \mathbf{B}_s(\dot{\mathbf{z}}_s - \dot{\mathbf{z}}_u) + \mathbf{u} = -\mathbf{K}_s(\mathbf{H}^T \mathbf{p} - \mathbf{z}_u) - \mathbf{B}_s(\mathbf{H}^T \dot{\mathbf{p}} - \dot{\mathbf{z}}_u) + \mathbf{u} \quad (11)$$

$$\begin{cases} \mathbf{M}_s \ddot{\mathbf{p}} = \mathbf{H} \mathbf{f} \\ \mathbf{M}_u \ddot{\mathbf{z}}_u = \mathbf{K}_t(\mathbf{z}_u - \mathbf{z}_r) - \mathbf{f} \end{cases} \quad (12)$$

$$\begin{cases} \mathbf{M}_s \ddot{\mathbf{p}} = -\mathbf{H} \mathbf{K}_s(\mathbf{H}^T \mathbf{p} - \mathbf{z}_u) - \mathbf{H} \mathbf{B}_s(\mathbf{H}^T \dot{\mathbf{p}} - \dot{\mathbf{z}}_u) + \mathbf{H} \mathbf{u} \\ \mathbf{M}_u \ddot{\mathbf{z}}_u = \mathbf{K}_s(\mathbf{H}^T \mathbf{p} - \mathbf{z}_u) + \mathbf{B}_s(\mathbf{H}^T \dot{\mathbf{p}} - \dot{\mathbf{z}}_u) + \mathbf{K}_t(\mathbf{z}_u - \mathbf{z}_r) - \mathbf{u} \end{cases} \quad (13)$$

$$\underbrace{\begin{bmatrix} \mathbf{M}_s & \mathbf{0}_{3 \times 4} \\ \mathbf{0}_{4 \times 3} & \mathbf{M}_u \end{bmatrix}}_{\mathbf{M}} \begin{bmatrix} \ddot{\mathbf{p}} \\ \ddot{\mathbf{z}}_u \end{bmatrix} = \underbrace{\begin{bmatrix} -\mathbf{H}\mathbf{K}_s\mathbf{H}^T & \mathbf{H}\mathbf{K}_s \\ \mathbf{K}_s\mathbf{H}^T & -\mathbf{K}_s + \mathbf{K}_f \end{bmatrix}}_{\mathbf{K}} \begin{bmatrix} \mathbf{p} \\ \mathbf{z}_u \end{bmatrix} + \underbrace{\begin{bmatrix} -\mathbf{H}\mathbf{B}_s\mathbf{H}^T & \mathbf{H}\mathbf{B}_s \\ \mathbf{B}_s\mathbf{H}^T & -\mathbf{B}_s \end{bmatrix}}_{\mathbf{B}} \begin{bmatrix} \dot{\mathbf{p}} \\ \dot{\mathbf{z}}_u \end{bmatrix} + \underbrace{\begin{bmatrix} \mathbf{H} \\ -\mathbf{I} \end{bmatrix}}_{\mathbf{U}} \mathbf{u} + \underbrace{\begin{bmatrix} \mathbf{0}_{3 \times 4} \\ -\mathbf{K}_f \end{bmatrix}}_{\mathbf{L}} \mathbf{w} \quad (14)$$

$$\mathbf{z} \triangleq \begin{bmatrix} \mathbf{p} \\ \mathbf{z}_u \end{bmatrix}, \quad \mathbf{x} \triangleq \begin{bmatrix} \mathbf{z} \\ \dot{\mathbf{z}} \end{bmatrix} \quad (15)$$

$$\mathbf{M}\ddot{\mathbf{z}} = \mathbf{K}\mathbf{z} + \mathbf{B}\dot{\mathbf{z}} + \mathbf{U}\mathbf{u} + \mathbf{L}\mathbf{w} \quad (16)$$

$$\begin{bmatrix} \dot{\mathbf{z}} \\ \ddot{\mathbf{z}} \end{bmatrix} = \begin{bmatrix} \mathbf{0}_{7 \times 7} & \mathbf{0}_{7 \times 7} \\ \mathbf{M}^{-1}\mathbf{K} & \mathbf{M}^{-1}\mathbf{B} \end{bmatrix} \begin{bmatrix} \mathbf{z} \\ \dot{\mathbf{z}} \end{bmatrix} + \begin{bmatrix} \mathbf{0}_{7 \times 4} \\ \mathbf{M}^{-1}\mathbf{L} \end{bmatrix} \mathbf{w} + \begin{bmatrix} \mathbf{0}_{7 \times 4} \\ \mathbf{M}^{-1}\mathbf{U} \end{bmatrix} \mathbf{u} \quad (17)$$

$$\dot{\mathbf{x}} = \underbrace{\begin{bmatrix} \mathbf{0}_{7 \times 7} & \mathbf{I}_{7 \times 7} \\ \mathbf{M}^{-1}\mathbf{K} & \mathbf{M}^{-1}\mathbf{B} \end{bmatrix}}_{\mathbf{A}} \mathbf{x} + \underbrace{\begin{bmatrix} \mathbf{0}_{7 \times 4} \\ \mathbf{M}^{-1}\mathbf{L} \end{bmatrix}}_{\mathbf{B}_1} \mathbf{w} + \underbrace{\begin{bmatrix} \mathbf{0}_{7 \times 4} \\ \mathbf{M}^{-1}\mathbf{U} \end{bmatrix}}_{\mathbf{B}_2} \mathbf{u} = \mathbf{A}\mathbf{x} + \mathbf{B}_1\mathbf{w} + \mathbf{B}_2\mathbf{u} \quad (18)$$

## 2.2. Design of LQR

When designing LQR, an LQ cost function needs to be defined. The LQ cost function,  $J$ , with the state variables is given as in Equation (19). The weights  $\zeta_i$  are determined by Bryson's rule, i.e.,  $\zeta_i = 1/\zeta_i^2$ , where  $\zeta_i$  is the maximum allowable value on each term [34]. For ride comfort improvement,  $\zeta_1$ ,  $\zeta_2$ , and  $\zeta_3$  ought to be set low. On the other hand, for road handling,  $\zeta_8$  and  $\zeta_9$  ought to be set low. Another objective of suspension control is to reduce motion sickness in this paper. According to recent studies, motion sickness is caused by combined vibrations along vertical and pitch directions in the 0.8~8.0 Hz frequency range [14,15]. For motion sickness reduction, the  $a_z$  and  $\dot{\theta}$  of an SPM ought to be reduced. For the purpose,  $\zeta_1$  and  $\zeta_7$  ought to be set lower.

The LQ cost function  $J$  is rewritten into Equation (20). The matrices  $\mathbf{Q}$ ,  $\mathbf{R}$  and  $\mathbf{N}$  are derived from the matrices  $\mathbf{A}$ ,  $\mathbf{B}_2$  and the weights in  $J$ . LQR is a full-state feedback controller, Equation (21), which minimizes  $J$ . It is easy to calculate the gain matrix of LQR,  $\mathbf{K}_{LQR}$ , from the solution of the Riccati equation,  $\mathbf{P}$ , for  $\mathbf{A}$ ,  $\mathbf{B}_2$ ,  $\mathbf{Q}$ ,  $\mathbf{R}$  and  $\mathbf{N}$ . The dimension of  $\mathbf{K}_{LQR}$  is  $4 \times 14$ , which is too large to implement on a real vehicle. Moreover, to implement  $\mathbf{K}_{LQR}$  on a real vehicle, 14 state variables should be measured or estimated by a state estimator. For this reason, it is very hard to implement  $\mathbf{K}_{LQR}$  on a real vehicle. To overcome this problem, a static output feedback (SOF) control is adopted in this paper.

$$J = \int_0^{\infty} \left\{ \zeta_1 \dot{z}_c^2 + \zeta_2 \dot{\phi}^2 + \zeta_3 \dot{\theta}^2 + \zeta_4 \phi^2 + \zeta_5 \dot{\phi}^2 + \zeta_6 \theta^2 + \zeta_7 \dot{\theta}^2 + \zeta_8 \sum_{i=1}^4 (z_{si} - z_{ui})^2 + \zeta_9 \sum_{i=1}^4 z_{ui}^2 + \zeta_{10} \sum_{i=1}^4 u_i^2 \right\} dt \quad (19)$$

$$J = \int_0^{\infty} \left\{ \begin{bmatrix} \mathbf{x} \\ \mathbf{u} \end{bmatrix}^T \begin{bmatrix} \mathbf{Q} & \mathbf{N} \\ \mathbf{N}^T & \mathbf{R} \end{bmatrix} \begin{bmatrix} \mathbf{x} \\ \mathbf{u} \end{bmatrix} \right\} dt \quad (20)$$

$$\mathbf{u} = -\mathbf{K}_{LQR}\mathbf{x} = -\mathbf{R}^{-1}\mathbf{B}_2^T\mathbf{P}\mathbf{x} \quad (21)$$

## 2.3. Sensor Signal Processing

A SOF controller uses available signals measured with sensors in a real vehicle. In this paper, the vertical velocity, the pitch, and the roll rates of the SPM are assumed to be available for SOF control. Those signals are obtained from four accelerometers located at the four corners of the SPM, i.e., ①, ②, ③ and ④, as shown in Figure 2 [35–37]. The signals measured from those accelerometers are filtered sequentially by high-pass and low-pass filters in order to reject noise and DC blocking, respectively. Those filters are given in Equations (22) and (23), respectively [17,35]. As pointed in the reference [35], Equation (22) plays a differentiator role below 0.1 Hz and an integrator role above 0.1 Hz, which excludes a possible DC offset. As a result, the vertical velocities at four corners of the SPM are

calculated. With those velocities, the vertical velocity, roll and pitch rates of the SPM are obtained by Equation (11). This procedure of sensor signal processing is shown in Figure 4.

$$\text{High-pass filter} = \frac{s}{s^2 + 2\zeta\omega_n s + \omega_n^2}, \quad \zeta = 0.707, \quad \omega_n = 0.1 \text{ Hz} \quad (22)$$

$$\text{Low-pass filter} = \frac{1}{\tau s + 1}, \quad \tau = 0.5\zeta\omega_l, \quad \zeta = 0.707, \quad \omega_l = 15 \sim 20 \text{ Hz} \quad (23)$$

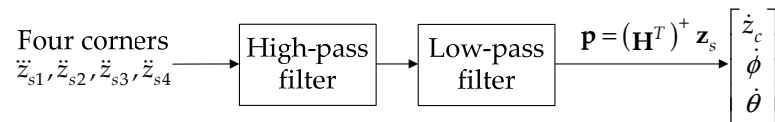


**Figure 4.** Block diagram for velocity and angular rate calculation.

#### 2.4. Design of SOF Controller with LQOC

Different from Figure 4, the vector of available outputs,  $\mathbf{y}$ , ought to be derived from the state vector  $\mathbf{x}$  and the matrices  $\mathbf{A}$ ,  $\mathbf{B}_1$  and  $\mathbf{B}_2$  for LQOC. The vector  $\mathbf{y}$  is defined from the state vector  $\mathbf{x}$  as in Equation (24). In this paper, three types of SOF controller are proposed. The first type of SOF controller is given in Equation (25). Since there are three sensor outputs and four control inputs, this type is natural when designing the SOF controller. As shown in Equation (25), there are twelve gains in  $\mathbf{K}_{SOF}$ . Let this controller be denoted as the SOF one.

$$\mathbf{y} = \begin{bmatrix} \dot{z}_c \\ \dot{\phi} \\ \dot{\theta} \end{bmatrix} = \mathbf{C}\mathbf{x} = \begin{bmatrix} \mathbf{0}_{3 \times 7} & \mathbf{I}_{3 \times 3} & \mathbf{0}_{3 \times 4} \end{bmatrix} \mathbf{x} \quad (24)$$

$$\mathbf{u} = \mathbf{K}_{SOF} \mathbf{y} = \begin{bmatrix} k_1 & k_2 & k_3 \\ k_4 & k_5 & k_6 \\ k_7 & k_8 & k_9 \\ k_{10} & k_{11} & k_{12} \end{bmatrix} \mathbf{y} \quad (25)$$

The second type of SOF controller is given in Equation (26). This type is called the structured SOF or SSOF controller. This type is based on the fact that there are symmetries between the front/rear and left/right suspensions, as shown in Figure 3 [28]. For this reason, the number of gains in  $\mathbf{K}_{SSOF}$  is three, which is much smaller than  $\mathbf{K}_{SOF}$ . The first column of  $\mathbf{K}_{SSOF}$  corresponds to the vertical control force. The second and third columns of  $\mathbf{K}_{SSOF}$  correspond to the roll and pitch moments, respectively. For this reason, the structure of  $\mathbf{K}_{SSOF}$  is identical to that of  $\mathbf{H}^T$  in Equation (7).

$$\mathbf{u} = \mathbf{K}_{SSOF} \mathbf{y} = \begin{bmatrix} k_1 & k_2 & k_3 \\ k_1 & -k_2 & k_3 \\ k_1 & k_2 & -k_3 \\ k_1 & -k_2 & -k_3 \end{bmatrix} \mathbf{y} \quad (26)$$

There are three motions in the SPM: VRP directions. If there are a vertical control force,  $F_{zc}$ , and roll and pitch moments,  $M_\phi$  and  $M_\theta$ , used to control the VRP motions independently, these can be transformed into four control inputs in  $\mathbf{u}$  with the matrix  $\mathbf{H}$ , as shown in Equations (5) and (27). This is called Lotus modal control [38–42]. In (27),  $\mathbf{H}^+$  is the pseudo-inverse of  $\mathbf{H}$ .  $F_{zc}$ ,  $M_\phi$  and  $M_\theta$  can be determined by several methods such as LQR, LQSOE and sliding mode control (SMC) [42]. In the previous study, two state variables are needed to calculate the control force and moments for each direction [42]. For this reason, six gains are needed to generate the control inputs. In this paper,  $F_{zc}$ ,  $M_\phi$  and  $M_\theta$  are simply calculated by multiplying the constant gain matrix,  $\mathbf{K}_{LSOF}$ , by the vector of the vertical velocity, the roll and pitch rates,  $\mathbf{y}$  [38]. This is a simple derivative control which combines the Lotus modal decomposition with Karnopp's skyhook damper [38]. Then, these three force/moments are converted into four control inputs at each corner with

$\mathbf{H}^+$ , as given in Equation (28). The number of gains in  $\mathbf{K}_{LSOF}$  is three, which is identical to  $\mathbf{K}_{SSOF}$ . This is the third type of SOF controller, called LSOF controller.

$$\begin{bmatrix} F_{zc} \\ M_\phi \\ M_\theta \end{bmatrix} = \mathbf{H}\mathbf{f} \Rightarrow \mathbf{u} = \mathbf{H}^+ \begin{bmatrix} F_{zc} \\ M_\phi \\ M_\theta \end{bmatrix} \quad (27)$$

$$\mathbf{u} = \mathbf{H}^+ \begin{bmatrix} F_{zc} \\ M_\phi \\ M_\theta \end{bmatrix} = \mathbf{H}^+ \mathbf{K}_{LSOF} \mathbf{y} = \mathbf{H}^+ \begin{bmatrix} k_1 & 0 & 0 \\ 0 & k_2 & 0 \\ 0 & 0 & k_3 \end{bmatrix} \mathbf{y} \quad (28)$$

The gain matrices  $\mathbf{K}_{SOF}$ ,  $\mathbf{K}_{SSOF}$  and  $\mathbf{K}_{LSOF}$  of the SOF controllers are optimized to minimize  $J$ . Those SOF controllers are called LQSOE, LQSSOF and LQLSOE controllers, respectively. To date, it has been shown that there are no analytical methods to optimize  $\mathbf{K}_{SOF}$  or  $\mathbf{K}_{SSOF}$  or  $\mathbf{K}_{LSOF}$  in terms of  $J$  [43]. Moreover, it has also been shown that there are no analytic methods to find an initial gain which stabilizes a given system. If one of  $\mathbf{K}_{SOF}$  or  $\mathbf{K}_{SSOF}$  or  $\mathbf{K}_{LSOF}$  is selected, let this be  $\mathbf{K}_s$ . With  $\mathbf{K}_s$ , the closed-loop system  $\mathbf{A}_c$  is calculated as in Equation (29). To optimize  $\mathbf{K}_s$ , the optimization problem is formulated as in Equation (30) [17,28,29]. In this paper, CMA-ES is applied as a HOM [31].

$$\mathbf{A}_c = \mathbf{A} + \mathbf{B}_2 \mathbf{K}_s \mathbf{C}, \quad \mathbf{K}_s \in [\mathbf{K}_{SOF}, \mathbf{K}_{SSOF}, \mathbf{K}_{LSOF}] \quad (29)$$

$$\begin{aligned} \min_{\mathbf{K}_s} \quad & \text{trace}(\mathbf{P}_s) \\ \text{s.t.} \quad & \begin{cases} \mathbf{P}_s = \mathbf{P}_s^T > \mathbf{0} \\ \max(\text{Re}[\mathbf{A}_c]) < 0 \\ \mathbf{A}_c^T \mathbf{P}_s + \mathbf{P}_s \mathbf{A}_c + \mathbf{Q} + \mathbf{C}^T \mathbf{K}_s^T \mathbf{N}^T + \mathbf{N} \mathbf{K}_s \mathbf{C} + \mathbf{C}^T \mathbf{K}_s^T \mathbf{R} \mathbf{K}_s \mathbf{C} = \mathbf{0} \end{cases} \end{aligned} \quad (30)$$

### 2.5. Design of SOF Controller with SLOM

The SOF controllers designed by LOQC, i.e., LQSOE, LQSSOF and LQLSOE controllers, are designed with the SSE of (18) and the LQ cost function of (19). Generally, the forces of springs and dampers are nonlinear with respect to the suspension stroke and suspension velocity in a real vehicle. If springs and dampers in the full-car model are nonlinear, the SSE cannot be derived. As a consequence, LOQC, (30), cannot be applied to design the LQSOE, LQSSOF and LQLSOE controllers.

To design three SOF controllers for nonlinear systems, a simulation optimization (SLOM) is applied in this paper [17,30]. Simulation optimization is a method to find an optimum solution through simulation on a target system [44,45]. For SLOM, the Simulink model is built from Equations (3) and (4), and the SOF controllers, Equations (25), (26) and (28). In the Simulink model, the springs and dampers are nonlinear. SLOM optimizes twelve elements in  $\mathbf{K}_{SOF}$  or three elements in  $\mathbf{K}_{SSOF}$  or  $\mathbf{K}_{LSOF}$  in terms of a certain cost function.

As mentioned earlier, the  $a_z$ ,  $\theta$  and  $\phi$  of an SPM ought to be reduced for ride comfort improvement and motion sickness reduction. For this purpose, the cost function of the SLOM,  $J_{SLOM}$ , is defined as in Equation (31) by combining these values. For a given particular gain matrix, each term in  $J_{SLOM}$  is obtained from a simulation carried out over the horizon  $T$  from  $t_0$  to  $t_1$ . In Equation (31),  $M$  is the conversion constant from radian to degree, i.e., 57.2957795, and  $\alpha$  and  $\beta$  are tuning parameters for  $\dot{\theta}$  and  $\dot{\phi}$ , respectively. Hereafter,  $\alpha$  and  $\beta$  are set to 0.1. For optimization, CMA-ES is applied [29,31]. When applying CMA-ES, no limits are imposed on each element in the gain matrices,  $\mathbf{K}_{SOF}$ ,  $\mathbf{K}_{SSOF}$  and  $\mathbf{K}_{LSOF}$ . The optimization procedure of the SLOM with CMA-ES is given in Figure 5. Let the SOF controllers, SOE, SSOF and LSOF, designed by SLOM be called SOSOF, SOSSOF and SOLSOE, respectively.

$$J_{SLOM} = \max(|\ddot{z}_c(T)|) + \alpha \cdot M \cdot \max(|\dot{\phi}(T)|) + \beta \cdot M \cdot \max(|\dot{\theta}(T)|), \quad T \in [t_0, t_1] \quad (31)$$

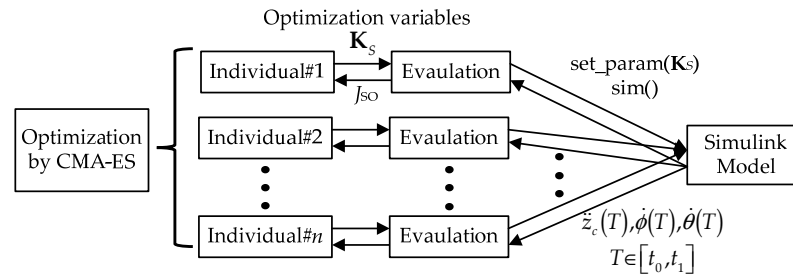


Figure 5. Optimization procedure of SLOM.

For SLOM, a road profile ought to be selected. In this paper, a twisted sine wave road (TSWR) is selected as a road profile, as given in Figure 6. TSWR has the period of 12.2 m and the amplitude of 0.05 m. In TWSR, the road profile on the right wheels is moved by the quarter period from that on the left ones. As a result, TSWR can simultaneously excite the VRP motions of the SPM. When using TSWR for SLOM, the vehicle speed is set to 15.0 m/s for the purpose of making severe conditions.

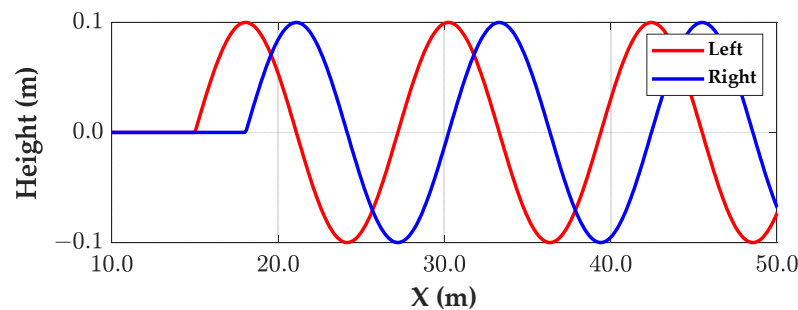


Figure 6. Twisted sine wave road profile for SLOM.

### 3. Simulation and Discussion

In this section, a simulation is carried out to evaluate the performance of six SOF controllers, LQSO, LQSSOF, LQLSO, SOSOF, SOSSOF and SOLSO. With the simulation results, those controllers are compared to one another in terms of ride comfort and motion sickness.

#### 3.1. Simulation Environment

Table 1 shows the parameters of the full-car model, which are references to an E-Class sedan given in CarSim [46]. The maximum allowable values in  $J$  are given in Table 2. As shown in Table 2, for ride comfort improvement and motion sickness reduction,  $\zeta_1$ ,  $\zeta_5$  and  $\zeta_7$ , were set low. This set tries to reduce the  $a_z$ ,  $\dot{\theta}$  and  $\dot{\phi}$  of an SPM. In this paper, the bandwidth of the actuator is assumed to be 20.0 Hz.

Table 1. Parameters of the full-car model [28].

$m_s$	1653.0 kg	$m_{u1}$	45.0 kg
$I_x$	614.0 kg·m <sup>2</sup>	$I_y$	2765.0 kg·m <sup>2</sup>
$l_f$	1.402 m	$l_r$	1.646 m
$t_f, t_r$	0.8 m	$k_t$	230,000.0 N/m
$k_s$	34,000.0 N/m	$b_s$	3500.0 N·s/m

Table 2. Maximum allowable values in LQ cost function.

$\zeta_1$	0.05 m/s <sup>2</sup>	$\zeta_2$	30.0 deg/s <sup>2</sup>	$\zeta_3$	30.0 deg/s <sup>2</sup>
$\zeta_4$	3.0 deg	$\zeta_5$	0.05 deg/s	$\zeta_6$	3.0 deg
$\zeta_7$	0.1 deg/s	$\zeta_8$	0.03 m	$\zeta_9$	0.03 m
$\zeta_{10}$	5000.0 N				

For SLOM, the force characteristic of nonlinear damper in the Simulink model are given in Figure 7. In CarSim, a linear spring was used, and its stiffness was set to 154,000.0 N/m. Those data were references to those of the E-Class sedan model given in CarSim.

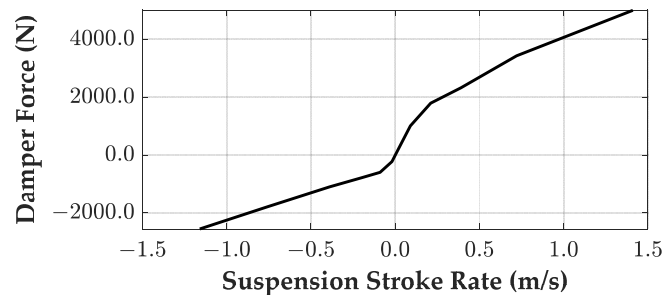


**Figure 7.** Damper force with respect to suspension stroke rate in the Simulink model.

As given in Section 2.5, SOSOF, SOSSOF and SOLSOF were designed with SLOM on MATLAB/Simulink. Six SOF controllers, LQSO, LQSSOF, LQLSOF, SOSOF, SOSSOF and SOLSOF, were implemented and simulated on a co-simulation environment built with MATLAB/Simulink and CarSim.

### 3.2. Simulation with the SOF Controllers Designed with LQOC

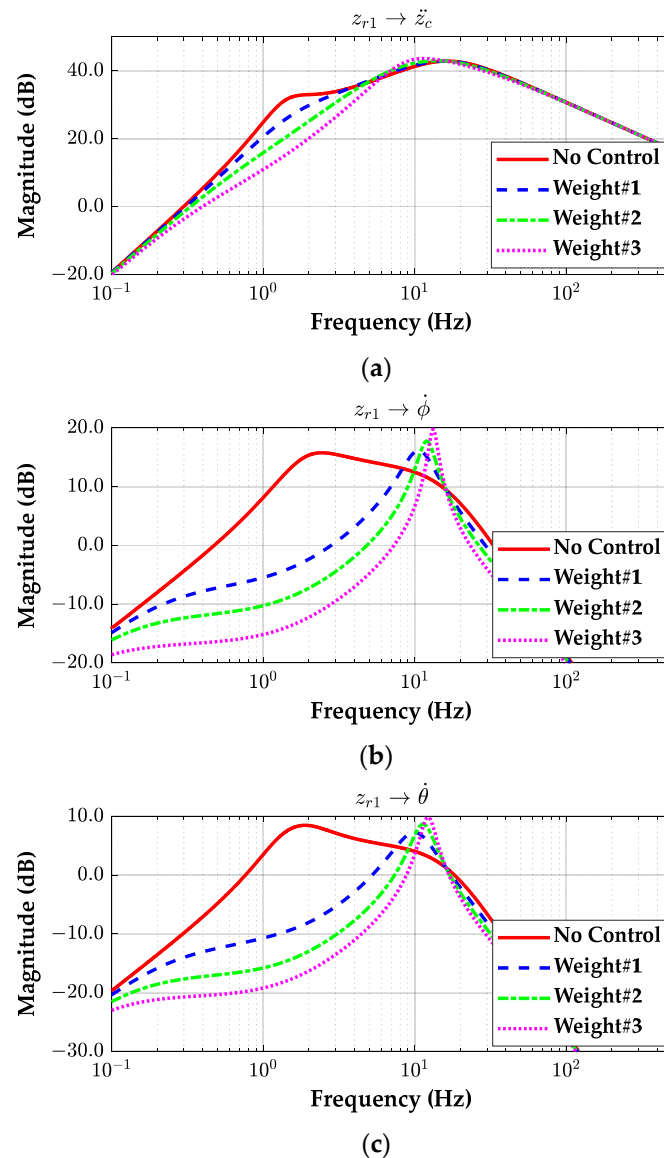
With the parameters and the weights given in Tables 1 and 2, the gain matrices of LQSO, LQSSOF and LQLSOF are given in Table 3. As shown in Table 3, those gain matrices are nearly identical to one another. This is a natural consequence because the structures of those controllers are nearly identical to one another and there are symmetries between the front/rear and left/right suspensions in view of the SPM. As a result, those controllers are expected to show equivalent performances to one another.

**Table 3.** Gain matrices from LQSO, LQSSOF and LQLSOF designed by LQOC.

$\mathbf{K}_{SOF}$	$\begin{bmatrix} -14,781.0 & -55,530.0 & 98,580.0 \\ -14,781.0 & 55,530.0 & 98,580.0 \\ -14,781.0 & -55,530.0 & -98,580.0 \\ -14,781.0 & 55,530.0 & -98,580.0 \end{bmatrix}$	$\mathbf{K}_{SSOF}$	$\begin{bmatrix} -16,002.0 & -55,530.0 & 82,021.0 \\ -16,002.0 & 55,530.0 & 82,021.0 \\ -13,630.0 & -55,530.0 & -82,021.0 \\ -13,630.0 & 55,530.0 & -82,021.0 \end{bmatrix}$
$\mathbf{G}^+\mathbf{K}_{LSOF}$	$\begin{bmatrix} -15,348.0 & -55,530.0 & 94,972.0 \\ -15,348.0 & 55,530.0 & 94,972.0 \\ -14,242.0 & -55,530.0 & -102,290.0 \\ -14,242.0 & 55,530.0 & -102,290.0 \end{bmatrix}$		

The performance of those SOF controllers can be improved by setting the maximum allowable values given in Table 2 smaller except  $\zeta_{10}$  on the control input. Generally,  $\zeta_{10}$  on the control input has a significant effect on the control performance. However, this has little effect on the control performance because it is very small. Instead,  $\zeta_1$ ,  $\zeta_5$  and  $\zeta_7$  should be set smaller. In the previous work, these values were not set small enough to give a better performance [17]. In this paper, these values were set much smaller than those in the previous work.

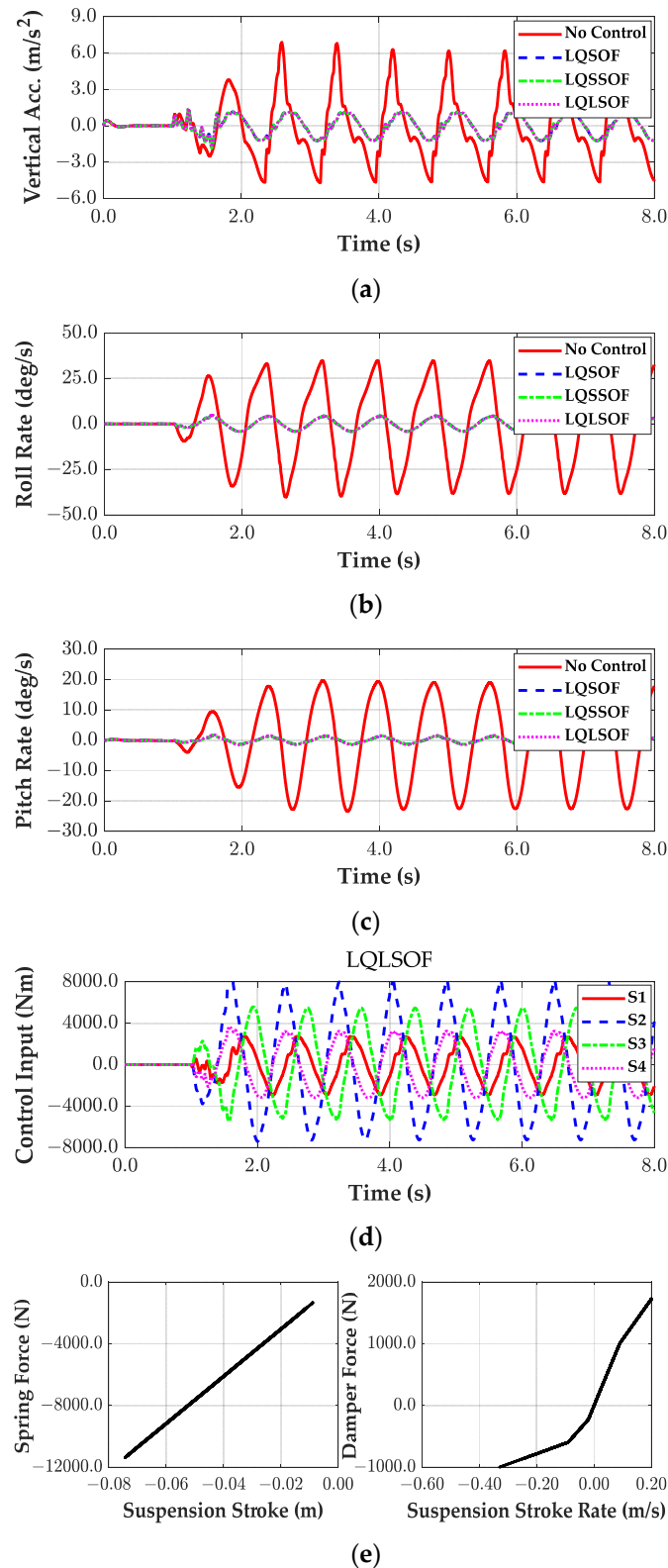
Let the LQLSOF controllers with the three sets of the maximum allowable values,  $(\zeta_1, \zeta_5, \zeta_7)$  of (0.2, 0.2, 0.2), (0.1, 0.1, 0.1) and (0.05, 0.05, 0.05) be denoted as Weight#1, Weight#2 and Weight#3, respectively. The other maximum allowable values are set as given in Table 2. Figure 8 shows the frequency responses of those three weight sets from the front left road profile,  $z_{r1}$ , to  $a_z$ ,  $\dot{\theta}$  and  $\dot{\phi}$  of an SPM. These responses are obtained with the SSE, Equation (18). As shown in Figure 8, the control performance is significantly improved as  $\zeta_1$ ,  $\zeta_5$  and  $\zeta_7$  are set smaller. From the results, it is recommended to set  $\zeta_1$ ,  $\zeta_5$  and  $\zeta_7$  as small as possible for ride comfort improvement and motion sickness reduction.



**Figure 8.** Frequency responses of the SOF controllers designed with LQOC and three sets of weights. (a) Vertical accelerations; (b) roll rates; (c) pitch rates.

Three SOF controllers, LQSOE, LQSSOF and LQLSOE, are simulated on a co-simulation environment with MATLAB/Simulink and CarSim. The controller gains given in Table 3 are used. The road profile used in CarSim is identical to that in Figure 6. The vehicle speed was set to 15 m/s and this is maintained as constant as possible by a speed controller.

Figure 9 shows the simulation results of those controllers designed with the weights given in Table 2. Table 4 summarizes the simulation results. As shown in Figure 9, those controllers show good performance in terms of ride comfort and motion sickness because  $a_z$  and  $\dot{\theta}$  are significantly decreased by those controllers. These results can be expected from the controller gains given in Table 3 and the frequency responses given in Figure 8. The spring and damper forces obtained from the simulation results of four cases coincide with those in Figure 7, as given in Figure 9e. As shown in Table 4, there are rare differences among those controllers in terms of the  $a_z$ ,  $\dot{\theta}$  and  $\dot{\phi}$  of the SPM. This is also expected from the controller gains given in Table 3. For this reason, only the control input of LQLSOE is given in Figure 9d.

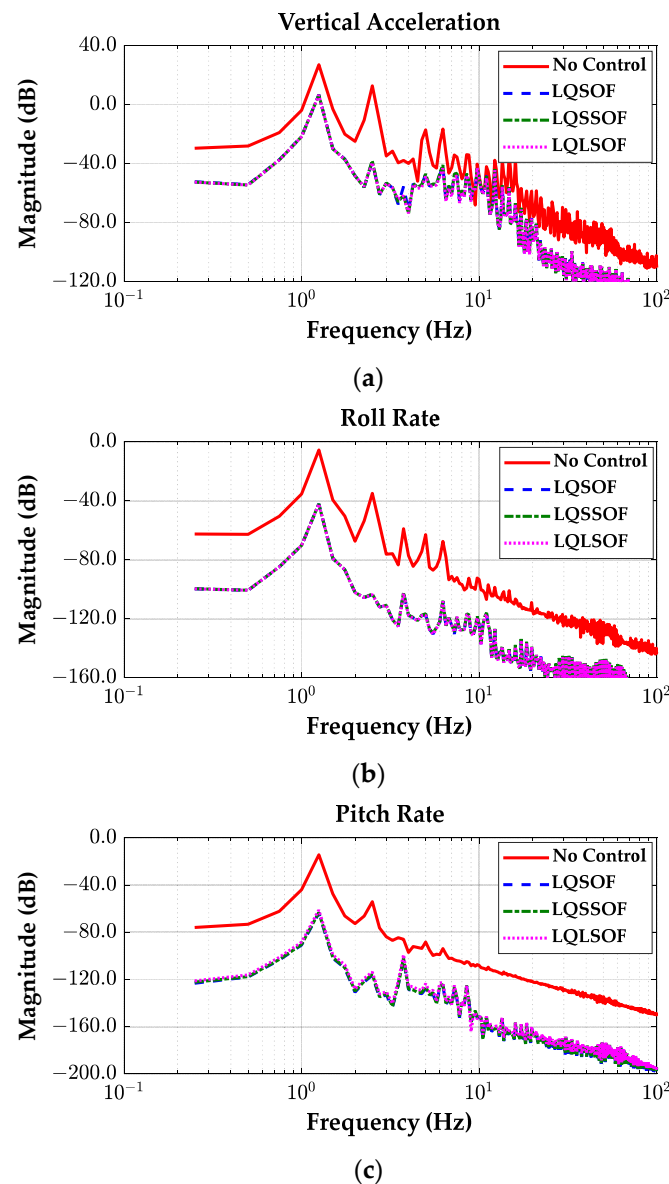


**Figure 9.** Simulation results of LQSO, LQSSOF and LQLSOF on the twisted sine wave road in CarSim. (a) Vertical accelerations; (b) roll rates; (c) pitch rates; (d) control inputs; (e) spring and damper forces.

**Table 4.** Summary of the simulation results of LQSO, LQSSOF and LQLSOF on CarSim.

Controller	Max $ \ddot{z}_c $ (m/s <sup>2</sup> )	Max $ \dot{\phi} $ (deg/s)	Max $ \dot{\theta} $ (deg/s)
No Control	6.9	40.3	23.4
LQSO	1.8	4.8	1.6
LQSSOF	1.8	4.8	1.7
LQLSOF	1.8	4.8	1.8

With the simulation results of the LQSO, LQSSOF and LQLSOF controllers, the frequency responses are obtained as given in Figure 10. As shown in Figure 10, the  $a_z$ ,  $\dot{\theta}$  and  $\dot{\phi}$  of an SPM were significantly reduced compared to the uncontrolled case below the frequency of 10 Hz. Especially important, the roll and pitch rates were reduced over the entire frequency range. These results mean that those three SOF controllers significantly improve ride comfort and motion sickness.

**Figure 10.** Frequency responses of LQSO, LQSSOF and LQLSOF on the twisted sine wave road. (a) Vertical accelerations; (b) roll rates; (c) pitch rates.

### 3.3. Simulation with SOF Controllers Designed by SLOM

Three SOF controllers, SOSOF, SOSSOF and SOLSOF, are designed by SLOM on MATLAB/Simulink. Different from the SOF controllers designed by LQOC, there are large differences among the gains of those controllers. Those controllers were simulated on a co-simulation environment with MATLAB/Simulink and CarSim.

Figure 11 shows the frequency responses of those controllers designed by SLOM on the TSWR. These plots were drawn with the SSE, as in Equation (18). As shown in Figure 11, SOSOF shows the best performance in terms of the roll and pitch rates. This is a natural consequence because SOSOF has twelve elements, which can cover a larger range of solution space than SSOF and LSOF. Figure 11b,c shows that there are a small differences between SOSOF and SOSSOF/SOLSOF. This is caused by the fact that there are no symmetries in SOSOF compared to SOSSOF and SOLSOF. In other words, the symmetries between the front/rear and left/right suspensions are not held for SOF. On the contrary, SSOF and LSOF have symmetries in their structures. As shown in Figure 11, the differences between SOSOF and SOSSOF/SOLSOF in terms of the pitch and roll rates are small, enough to be neglected because SOSSOF/SOLSOF shows quite good performance in controlling the pitch and roll motions of the SPM. For this reason, SOF is not recommended as a controller in terms of the number of gain elements.

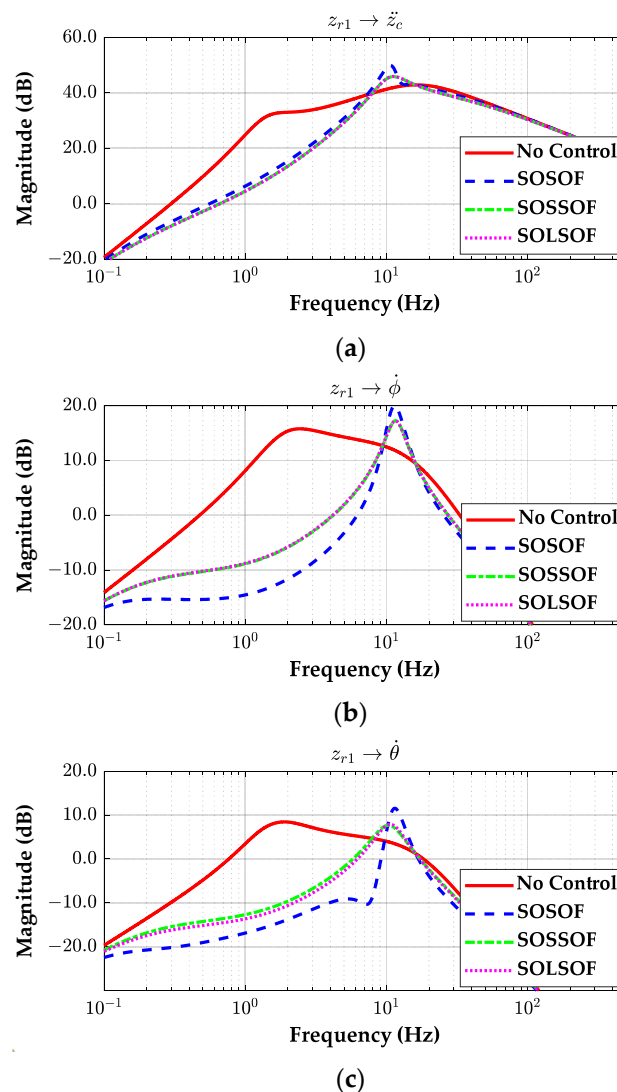


**Figure 11.** Frequency responses of SOSOF, SOSSOF and SOLSOF designed with SLOM on TSWR. (a) Vertical accelerations; (b) roll rates; (c) pitch rates.

Three SOF controllers designed by SLOM, i.e., SOSOF, SOSSOF and SOLSOF controllers, were simulated on CarSim. The road profile used in CarSim is identical to that of Figure 6. The vehicle speed was set to 15 m/s and this is maintained as constant as possible by a speed controller in CarSim.

Figure 12 shows the simulation results of SOSOF, SOSSOF and SOLSOF on CarSim. Table 5 summarizes the simulation results of those controllers. As expected from Figure 11, those controllers show good performance in terms of  $a_z$ ,  $\theta$  and  $\dot{\phi}$  of an SPM. However, as shown in Figure 12a, there is chattering in the vertical acceleration of SOLSOF, which cannot be applied to real vehicles. This is caused by large gains, which means large damping or derivative control. To remove this chattering,  $\alpha$  and  $\beta$  in  $J_{SO}$  should be tuned finely. As shown in Table 5, there are differences in the three measures for each controller. On the contrary, the controllers, LQSOF, LQSSOF and LQLSOF, show nearly identical and consistent results, as shown in Table 4. This is caused by the cost function  $J_{SO}$  of SLOM. If  $\alpha$  and  $\beta$  in  $J_{SO}$  are tuned finely, then the SOSSOF and SOLSOF controllers can give better results than the LQSOF, LQSSOF and LQLSOF ones.

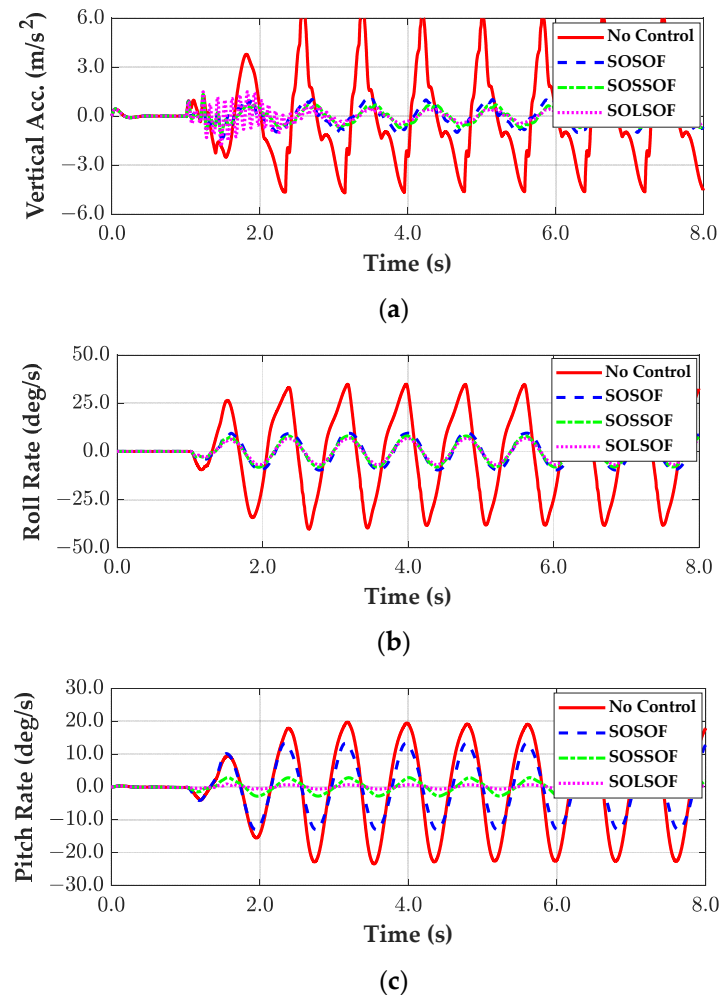
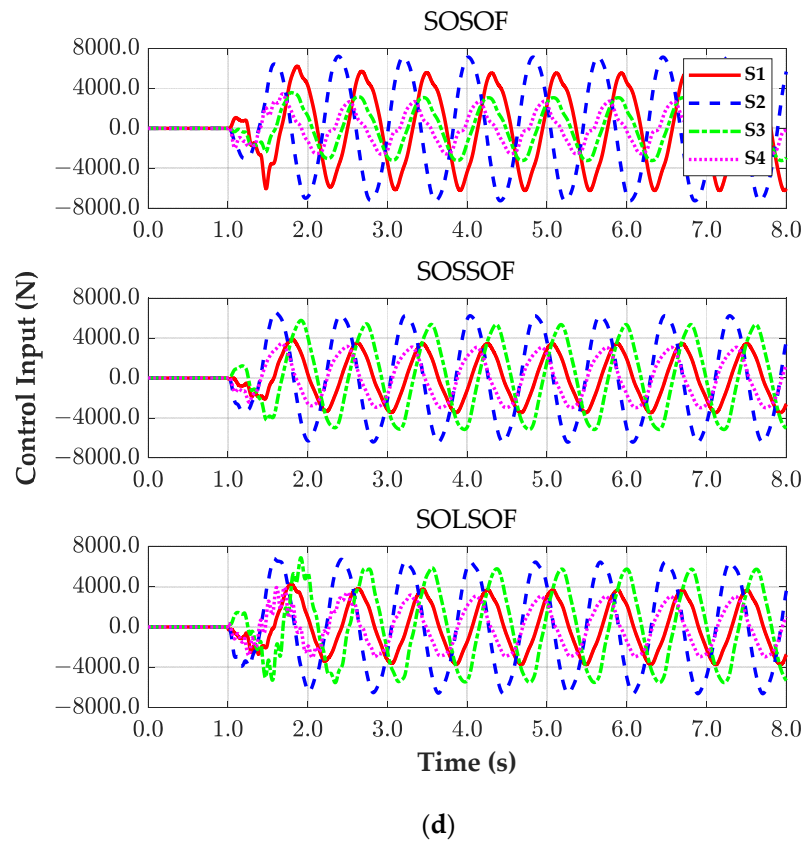


Figure 12. Cont.



**Figure 12.** Simulation results of SOSOF, SOSSOF and SOLSOF on the TSWR in CarSim. (a) Vertical accelerations; (b) roll rates; (b) pitch rates; (d) control inputs.

**Table 5.** Summary of the simulation results of SOSOF, SOSSOF and SOLSOF on CarSim.

Controller	Max $ \ddot{z}_c $ (m/s <sup>2</sup> )	Max $ \dot{\phi} $ (deg/s)	Max $ \dot{\theta} $ (deg/s)
No Control	6.9	40.3	23.4
SOSOF	1.4	9.8	13.3
SOSSOF	1.3	8.2	2.8
SOLSOF	1.9	7.0	0.9

With the simulation results of the SOSOF, SOSSOF and SOLSOF controllers, the frequency responses are obtained as given in Figure 13. As shown in Figure 13, SOLSOF shows the best performance, and SOSOF shows the worst performance. These results mean that SOLSOF is recommended as a suspension controller for ride comfort improvement and motion sickness reduction under the condition that it is tuned finely. In view of computation time, the SOF controllers designed by LQOC are superior to those designed by SLOM because SLOM requires a larger amount of computation time than LQOC. Moreover, by comparing the results given in Tables 4 and 5, SOF controllers designed by LQOC are recommended as a suspension controller for ride comfort improvement and motion sickness reduction.

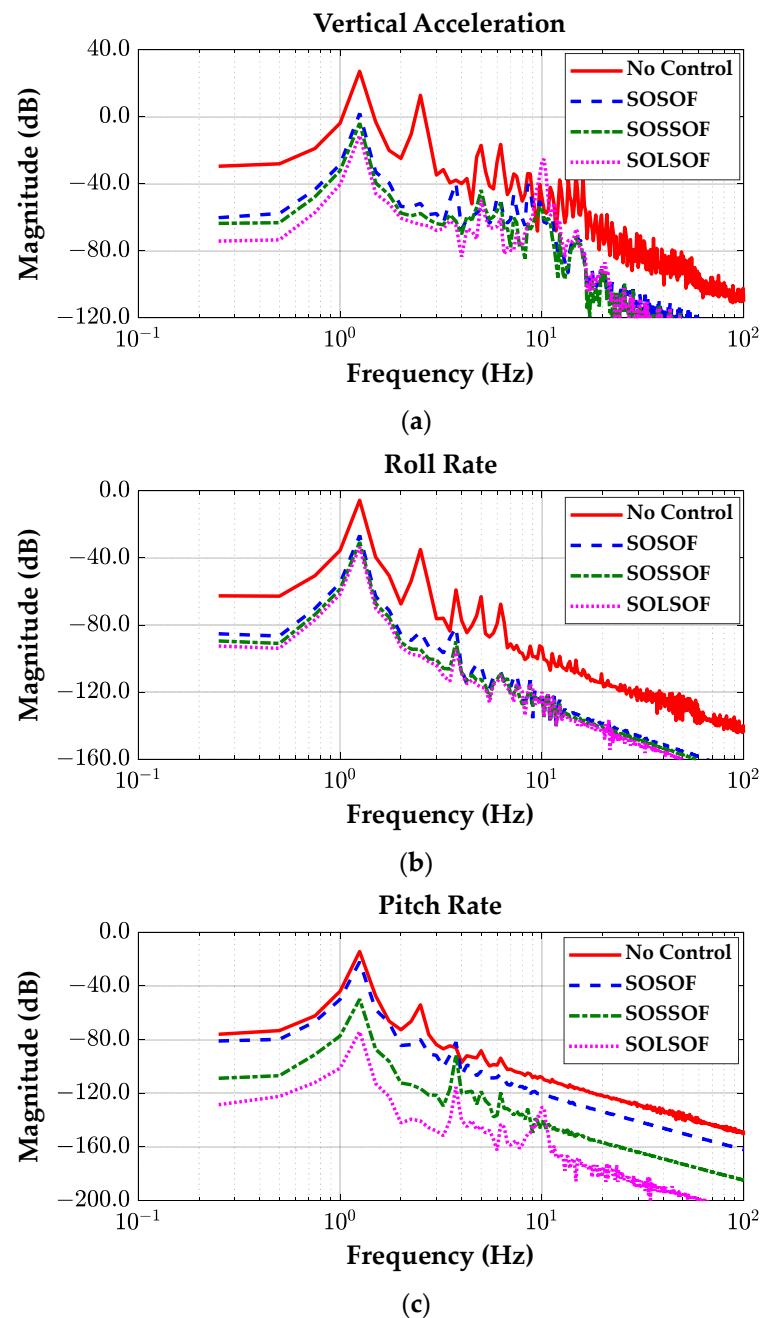


**Figure 13.** Frequency responses of SOSOF, SOSSOF and SOLSOF on the twisted sine wave road. (a) Vertical accelerations; (b) roll rates; (c) pitch rates.

#### 4. Conclusions

This paper presented a method to design static output feedback active suspension controllers for ride comfort improvement and motion sickness reduction. The vertical velocity, and the roll and pitch rates were obtained with filters from the accelerometers located at the corners of the SPM. With these signals, three types of SOF controllers were presented. Among them, two SOF controllers were derived from the symmetries between the front/rear and left/right suspensions. These two controllers have three gains despite four control inputs being used in the full-car model, which is much smaller than the 56 gain elements of LQR. Those SOF controllers were optimized with LQOC and SLOM. To check the performance of the proposed SOF controllers, frequency response analysis was carried out with the SSE of the full-car model and a simulation was performed on CarSim. Based on the simulation results, it was shown that the proposed SOF controllers

with three gains significantly improved the control performance in terms of ride comfort and motion sickness by reducing the vertical acceleration, and the roll and pitch rates of the sprung mass. From the experimental results, it was verified that the sensor signals for SOF controllers can be obtained from the accelerometers located at corners the SPM, and that the accelerometers on the wheel centers are not needed. In view of this controller design methodology, with the SOF controller structure, LQOC is preferred to SLOM because the former is more systematic than the latter and the latter is more case-dependent than the former. Moreover, the former can generate more consistent results than the latter regardless of vehicle type, parameters, and road profiles. For those reasons, the SOF controllers calculated with LQOC can be used as a starting point in experiments on real vehicles. This was confirmed by the experimental results. In further research, an experimental investigation will be carried out with the proposed controller on real vehicles, and the experimental results will be given within 6 months.

**Author Contributions:** Conceptualization, J.K. and S.Y.; methodology, S.Y.; software, S.Y.; validation, J.K. and S.Y.; formal analysis, S.Y.; investigation, J.K. and S.Y.; resources, S.Y.; data curation, S.Y.; writing—original draft preparation, S.Y.; writing—review and editing, J.K.; visualization, J.K. and S.Y.; supervision, S.Y.; funding acquisition, S.Y. All authors have read and agreed to the published version of the manuscript.

**Funding:** This work was supported by the Ministry of Education through the National Research Foundation of Korea (NRF) under Basic Science Research Program (NRF-2019R1A6A1A03032119).

**Data Availability Statement:** No new data were created or analyzed in this study. Data sharing is not applicable to this article.

**Conflicts of Interest:** The authors declare no conflicts of interest.

## Nomenclature

ASC	active suspension control
HOM	heuristic optimization method
LQOC	linear quadratic optimal control
LQR	linear quadratic regulator
LQSO	linear quadratic static output feedback
LQSSOF	linear quadratic structured static output feedback
LQLSOF	linear quadratic Lotus modal static output feedback
LSOF	Lotus modal static output feedback control
SLOM	simulation optimization method
SOF	static output feedback
SPM	sprung mass or vehicle body
SSE	state-space equation
SSOF	structured static output feedback
TSWR	twisted sine wave road
USPM	unsprung mass or tire
$a_z = \ddot{z}_c$	vertical acceleration of a sprung mass (m/s <sup>2</sup> )
$b_{si}$	damping coefficient of a damper at $i$ -th suspension (N·s/m)
$I_x, I_y$	roll and pitch moments of inertia (kg·m <sup>2</sup> )
$J$	LQ cost function of LQR
$J_{SO}$	Cost function of SLOM
$k_{si}$	spring stiffness of a spring at $i$ -th suspension (N/m)
$k_{ti}$	spring stiffness of $i$ -th tire (N/m)
$l_f, l_r$	distances from center of gravity of a sprung mass to front and rear axles (m)
$m_s$	sprung mass (kg)
$m_{ui}$	unsprung mass under $i$ -th suspension (kg)
$t_f, t_r$	half of track widths of front and rear axles (m)
$T, t_0, t_1$	simulation horizon from the start time $t_0$ to the end time $t_1$
$u_i$	forces generated by an actuator at $i$ -th suspension (N)
$v_z = \dot{z}_c$	vertical velocity of SPM (m/s)

$z_c$	heave displacement at center of gravity of a sprung mass (m)
$z_{ri}$	road elevation acting on $i$ -th tire (m)
$z_{si}$	vertical displacement of $i$ -th corners of a sprung mass (m)
$z_{wi}$	vertical displacement of $i$ -th wheel center (m)
$\xi_i$	maximum allowable value of weight in LQ cost function
$\zeta_i$	weight in LQ cost function
$\phi, \dot{\phi}$	roll angle and rate of a sprung mass (rad, rad/s)
$\theta, \dot{\theta}$	pitch angle and rate of a sprung mass (rad, rad/s)

## References

- Hrovat, D. Survey of advanced suspension developments and related optimal control applications. *Automatica* **1997**, *33*, 1781–1817. [CrossRef]
- Tseng, H.E.; Hrovat, D. State of the art survey: Active and semi-active suspension control. *Veh. Syst. Dyn.* **2015**, *53*, 1034–1062. [CrossRef]
- ISO 2631-1; Mechanical Vibration and Shock—Evaluation of human exposure to whole-body vibration—Part 1: General requirements. International Organization for Standardization: Geneva, Switzerland, 1997.
- Rimell, A.N.; Mansfield, N.J. Design of digital filters for frequency weightings required for risk assessments of workers exposed to vibration. *Ind. Health* **2007**, *45*, 512–519. [CrossRef]
- Yurtsever, E.; Lambert, J.; Carballo, A.; Takeda, K. A survey of autonomous driving: Common practices and emerging technologies. *IEEE Access* **2020**, *8*, 58443–58469. [CrossRef]
- Diels, C.; Bos, J.E. Self-driving carsickness. *Appl. Ergon.* **2016**, *53*, 374–382. [CrossRef] [PubMed]
- Asua, E.; Gutiérrez-Zaballa, J.; Mata-Carballeira, O.; Ruiz, J.A.; del Campo, I. Analysis of the motion sickness and the lack of comfort in car passengers. *Appl. Sci.* **2022**, *12*, 3717. [CrossRef]
- Xie, W.; He, D.; Wu, G. Inducers of motion sickness in vehicles: A systematic review of experimental evidence and meta-analysis. *Transp. Res. Part F Traffic Psychol. Behav.* **2023**, *99*, 167–188. [CrossRef]
- Lawther, A.; Griffin, M.J. A survey of the occurrence of motion sickness amongst passengers at sea. *Aviat. Space Environ. Med.* **1988**, *59*, 399–406.
- Griffin, M.; Newman, M. An experimental study of low-frequency motion in cars. *Proc. Inst. Mech. Eng. Part D J. Automob. Eng.* **2004**, *218*, 1231–1238. [CrossRef]
- Griffin, M.J.; Newman, M.M. Visual field effects on motion sickness in cars. *Aviat. Space Environ. Med.* **2004**, *75*, 739–748.
- Griffin, M.J.; Mills, K.L. Effect of frequency and direction of horizontal oscillation on motion sickness. *Aviat. Space Environ. Med.* **2002**, *73*, 537–543.
- Donohew, B.E.; Griffin, M.J. Motion sickness: Effect of the frequency of lateral oscillation. *Aviat. Space Environ. Med.* **2004**, *75*, 649–656. [PubMed]
- Ekchian, J.; Graves, W.; Anderson, Z.; Giovanardi, M.; Godwin, O.; Kaplan, J.; Ventura, J.; Lackner, J.R.; DiZio, P. *A High-Bandwidth Active Suspension for Motion Sickness Mitigation in Autonomous Vehicles*; SAE Technical Paper 2016-01-1555; SAE International: Warrendale, PA, USA, 2016.
- DiZio, P.; Ekchian, J.; Kaplan, J.; Ventura, J.; Graves, W.; Giovanardi, M.; Anderson, Z.; Lackner, J.R. An active suspension system for mitigating motion sickness and enabling reading in a car. *Aerosp. Med. Hum. Perform.* **2018**, *89*, 822–829. [CrossRef] [PubMed]
- Koohestani, A.; Nahavandi, D.; Asadi, H.; Kebria, P.M.; Khosravi, A.; Alizadehsani, R.; Nahavandi, S. A knowledge discovery in motion sickness: A comprehensive literature review. *IEEE Access* **2019**, *7*, 85755–85770. [CrossRef]
- Jeong, Y.; Yim, S. Design of active suspension controller for ride comfort enhancement and motion sickness mitigation. *Machines* **2024**, *12*, 254. [CrossRef]
- Sharp, R.S.; Crolla, D.A. Road vehicle suspension system design—A review. *Veh. Syst. Dyn.* **1987**, *16*, 167–192. [CrossRef]
- Cao, D.; Song, X.; Ahmadian, M. Editors' perspectives: Road vehicle suspension design, dynamics, and control. *Veh. Syst. Dyn.* **2011**, *49*, 3–28. [CrossRef]
- Theunissen, J.; Tota, A.; Gruber, P.; Dhaens, M.; Sorniotti, A. Preview-based techniques for vehicle suspension control: A state-of-the-art review. *Annu. Rev. Control* **2021**, *51*, 206–235. [CrossRef]
- Al-Ashmori, M.; Wang, X. A systematic literature review of various control techniques for active seat suspension systems. *Appl. Sci.* **2020**, *10*, 1148. [CrossRef]
- Wilson, D.A.; Sharp, R.S.; Hassan, S.A. The application of linear optimal control theory to the design of active automobile suspensions. *Veh. Syst. Dyn.* **1987**, *15*, 105–118. [CrossRef]
- Hac, A. Optimal linear preview control of active vehicle suspension. *Veh. Syst. Dyn.* **1992**, *21*, 167–195. [CrossRef]
- Abdel-Hady, M.B.A.; Crolla, D.A. Active suspension control algorithms for a four wheel vehicle model. *Int. J. Veh. Des.* **1992**, *13*, 144–158.
- Mudduluru, S.R.; Chizari, M. Quarter and full car models optimisation of passive and active suspension system using genetic algorithm. *arXiv* **2021**, arXiv:2101.12629. Available online: <https://arxiv.org/abs/2101.12629> (accessed on 30 August 2021).
- Camino, J.F.; Zampieri, D.E.; Peres, P.L.D. Design of a vehicular suspension controller by static output feedback. In Proceedings of the American Control Conference, San Diego, CA, USA, 2–4 June 1999; pp. 3168–3171.

27. Elmadany, M.M.; Al-Majed, M.I. Quadratic synthesis of active controls for a quarter-car model. *J. Vib. Control* **2001**, *7*, 1237–1252. [[CrossRef](#)]
28. Park, M.; Yim, S. Design of static output feedback and structured controllers for active suspension with quarter-car model. *Energies* **2021**, *14*, 8231. [[CrossRef](#)]
29. Jeong, Y.; Shon, Y.; Chang, S.; Yim, S. Design of static output feedback controllers for an active suspension system. *IEEE Access* **2022**, *10*, 26948–26964. [[CrossRef](#)]
30. Jeong, Y.; Shon, Y.; Chang, S.; Yim, S. Design of virtual reference feedforward controller for an active suspension system. *IEEE Access* **2022**, *10*, 65671–65684. [[CrossRef](#)]
31. Hansen, N.; Muller, S.D.; Koumoutsakos, P. Reducing the time complexity of the derandomized evolution strategy with covariance matrix adaptation (CMA-ES). *Evol. Comput.* **2003**, *11*, 1–18. [[CrossRef](#)]
32. Lu, J.; DePoyster, M. Multiobjective optimal suspension control to achieve integrated ride and handling performance. *IEEE Trans. Control Syst. Technol.* **2002**, *10*, 807–821.
33. Jung, Y.H.; Choi, J.W.; Seo, Y.B. Overlapping decentralized EA control design for an active suspension system of a full car model. In Proceedings of the 39th SICE Annual Conference, Iizuka, Japan, 28 July 2000; pp. 85–90.
34. Bryson, A.E., Jr.; Ho, Y. *Applied Optimal Control*; Hemisphere: New York, NY, USA, 1975.
35. Hong, K.; Sohn, H.; Hedrick, J.K. Modified skyhook control of semi-active suspensions: A new model, gain scheduling, and hardware-in-the-loop tuning. *J. Dyn. Syst. Meas. Control* **2002**, *124*, 158–167. [[CrossRef](#)]
36. Ding, R.; Wang, R.; Meng, X.; Chen, L. Energy consumption sensitivity analysis and energy-reduction control of hybrid electromagnetic active suspension. *Mech. Syst. Signal Process.* **2019**, *134*, 106301. [[CrossRef](#)]
37. Liu, W.; Wang, R.; Ding, R.; Meng, X.; Yang, L. On-line estimation of road profile in semi-active suspension based on unsprung mass acceleration. *Mech. Syst. Signal Process.* **2020**, *135*, 106370. [[CrossRef](#)]
38. Ikenaga, S.; Lewis, F.L.; Campos, J.; Davis, L. Active suspension control of ground vehicle based on a full-vehicle model. In Proceedings of the American Control Conference, Chicago, IL, USA, 28–30 June 2000.
39. Demic, M.; Diligenski, D.; Demic, I.; Demic, M. A method of vehicle active suspension design. *Forsch Ingenieurwes* **2006**, *70*, 145–158. [[CrossRef](#)]
40. Braghin, F.; Resta, F.; Sabbioni, E. A modal control for active/semi-active suspension systems. In Proceedings of the 2007 IEEE/ASME International Conference on Advanced Intelligent Mechatronics, Zurich, Switzerland, 4–7 September 2007.
41. Enders, E.; Karle, P.; Bonelli, G.; Killian, D.; Burkhard, G. Modal vertical vehicle dynamics control for semi-active and active suspension systems. In Proceedings of the 2020 Fifteenth International Conference on Ecological Vehicles and Renewable Energies (EVER), Monte-Carlo, Monaco, 10–12 September 2020.
42. Park, M.; Jeong, Y.; Yim, S. Design of a modal controller with simple models for an active suspension system. *IEEE Access* **2022**, *10*, 65585–65597. [[CrossRef](#)]
43. Syrmos, V.L.; Abdallah, C.T.; Dorato, P.; Grigoriadis, K. Static output feedback—A survey. *Automatica* **1997**, *33*, 125–137. [[CrossRef](#)]
44. Andradóttir, S. Chapter 20 An Overview of Simulation Optimization via Random Search. *Handb. Oper. Res. Manag. Sci.* **2006**, *13*, 617–631.
45. Amaran, S.; Sahinidis, N.V.; Sharda, B.; Bury, S.J. Simulation optimization: A review of algorithms and applications. *Ann. Oper. Res.* **2016**, *240*, 351–380. [[CrossRef](#)]
46. Mechanical Simulation Corporation. *CarSim Data Manual*; Version 8; Mechanical Simulation Corporation: Ann Arbor, MI, USA, 2009.

**Disclaimer/Publisher’s Note:** The statements, opinions and data contained in all publications are solely those of the individual author(s) and contributor(s) and not of MDPI and/or the editor(s). MDPI and/or the editor(s) disclaim responsibility for any injury to people or property resulting from any ideas, methods, instructions or products referred to in the content.